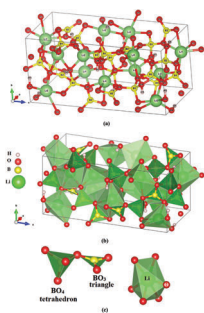


We have presented the Graphical Abstract text and image for your article below. This brief summary of your work will appear in the contents pages of the issue in which your article appears.



**Lithium borate  $\text{Li}_3\text{B}_5\text{O}_8(\text{OH})_2$  with large second harmonic generation and a high damage threshold in the deep-ultraviolet spectral range**

Q1

A. H. Reshak

The electronic structure and linear and nonlinear optical susceptibility dispersions of lithium borate  $\text{Li}_3\text{B}_5\text{O}_8(\text{OH})_2$  are comprehensively investigated.

Q3

Please check this proof carefully. **Our staff will not read it in detail after you have returned it.**

**Proof corrections must be returned as a single set of corrections, approved by all co-authors.** No further corrections can be made after you have submitted your proof corrections as we will publish your article online as soon as possible after they are received.

Please ensure that:

- The spelling and format of all author names and affiliations are checked carefully. Names will be indexed and cited as shown on the proof, so these must be correct.
- Any funding bodies have been acknowledged appropriately.
- All of the editor's queries are answered.
- Any necessary attachments, such as updated images or ESI files, are provided.

Translation errors between word-processor files and typesetting systems can occur so the whole proof needs to be read. Please pay particular attention to: tables; equations; numerical data; figures and graphics; and references.

Please send your corrections preferably as a copy of the proof PDF with electronic notes attached or alternatively as a list of corrections – do not change the text within the PDF file or send a revised manuscript. Corrections at this stage should be minor and not involve extensive changes.

Please return your **final** corrections, where possible within **48 hours** of receipt, by e-mail to: pccp@rsc.org. If you require more time, please notify us by email.

## Funder information

Providing accurate funding information will enable us to help you comply with your funders' reporting mandates. Clear acknowledgement of funder support is an important consideration in funding evaluation and can increase your chances of securing funding in the future. We work closely with Crossref to make your research discoverable through the Funding Data search tool (<http://search.crossref.org/funding>).

Further information on how to acknowledge your funders can be found on our webpage (<http://rsc.li/funding-info>).

### What is Funding Data?

Funding Data (<http://www.crossref.org/fundingdata/>) provides a reliable way to track the impact of the work that funders support. We collect funding information from our authors and match this information to funders listed in the Crossref Funder Registry. Once an article has been matched to its funders, it is discoverable through Crossref's search interface.

### PubMed Central

Accurate funder information will also help us identify articles that are mandated to be deposited in PubMed Central (PMC) and deposit these on your behalf.

## Providing funder information

We have combined the information you gave us on submission with the information in your acknowledgements. This will help ensure funding information is as complete as possible and matches funders listed in the Crossref Funder Registry. **Please check that the funder names and grant numbers in the table are correct.** This table will not be included in your final PDF but we will share the data with Crossref so that your article can be found *via* the Funding Data search tool.

Funder name	Funder ID (for RSC use only)	Award/grant/contract number
European Regional Development Fund	501100008530	Unassigned
Ministerstvo Školství, Mládeže a Tělovýchovy	501100001823	Unassigned

Q2

If a funding organisation you included in your acknowledgements or on submission of your article is not currently listed in the registry it will not appear in the table above. We can only deposit data if funders are already listed in the Crossref Funder Registry, but we will pass all funding information on to Crossref so that additional funders can be included in future.

## Researcher information

If any authors have ORCID or ResearcherID details that are not listed below, please provide these with your proof corrections. Please check that the ORCID and ResearcherID details listed below have been assigned to the correct author. Authors should have their own unique ORCID iD and should not use another researcher's, as errors will delay publication.

Please also update your account on our online manuscript submission system to add your ORCID details, which will then be automatically included in all future submissions. See [here](#) for step-by-step instructions and more information on author identifiers.

First (given) name(s)	Last (family) name(s)	ResearcherID	ORCID
A. H.	Reshak		0000-0001-9426-8363

## Queries for the attention of the authors

Journal: PCCP






Paper: c7cp06006h

Title: **Lithium borate  $\text{Li}_3\text{B}_5\text{O}_8(\text{OH})_2$  with large second harmonic generation and a high damage threshold in the deep-ultraviolet spectral range**

For your information: You can cite this article before you receive notification of the page numbers by using the following format: (authors), Phys. Chem. Chem. Phys., (year), DOI: 10.1039/c7cp06006h.

Editor's queries are marked on your proof like this **Q1**, **Q2**, etc. and for your convenience line numbers are indicated like this 5, 10, 15, ...

Please ensure that all queries are answered when returning your proof corrections so that publication of your article is not delayed.

Query reference	Query	Remarks
Q1	Please carefully check the spelling of all author names. This is important for the correct indexing and future citation of your article. No late corrections can be made.	
Q2	Funder details have been incorporated in the funder table using information provided in the article text. Please check that the funder information in the table is correct.	
Q3	Please check that the inserted Graphical Abstract image and text are suitable. Please ensure that the text fits between the two horizontal lines.	
Q4	The sentence beginning "They reported that the..." has been altered for clarity, please check that the meaning is correct.	
Q5	Ref. 52: Please provide the year of publication.	

# Lithium borate $\text{Li}_3\text{B}_5\text{O}_8(\text{OH})_2$ with large second harmonic generation and a high damage threshold in the deep-ultraviolet spectral range†

Cite this: DOI: 10.1039/c7cp06006h

A. H. Reshak 

The electronic structure and linear and nonlinear optical susceptibility dispersions of lithium borate  $\text{Li}_3\text{B}_5\text{O}_8(\text{OH})_2$  are comprehensively investigated. The investigation is achieved on  $\text{Li}_3\text{B}_5\text{O}_8(\text{OH})_2$  in the form of single crystals, taking into account the influence of the packing of the structural units on the linear and nonlinear optical susceptibility dispersion. The calculations highlight that the  $\text{BO}_3$  structural unit packing is the main source of the large birefringence in  $\text{Li}_3\text{B}_5\text{O}_8(\text{OH})_2$  due to the high anisotropic electron distribution, and, hence, it affects the macroscopic second harmonic generation (SHG) coefficients. This work provides a new path for the design of UV-NLO materials with high SHG efficiencies and short cutoff edges by introducing an alkali metal into borates. The large SHG is due to hyperpolarizability formed by co-parallel  $\text{BO}_3$  triangle groups. The absorption edge of  $\text{Li}_3\text{B}_5\text{O}_8(\text{OH})_2$  occurs at  $\lambda = 190$  nm and the optical band gap is estimated to be 6.52 eV, which is in good agreement with the experimental data (6.526 eV). The energy gap value confirms that  $\text{Li}_3\text{B}_5\text{O}_8(\text{OH})_2$  exhibits an exceptional laser damage threshold and is expected to produce coherent radiation in the deep-ultraviolet (DUV) region. The obtained value of SHG at  $\lambda = 1064$  nm is about 1.5 times that of the well-known NLO crystal  $\text{KH}_2\text{PO}_4$  (KDP) at  $\lambda = 1064$  nm and 3.5 times that of KDP at  $\lambda = 190$  nm, which is transparent down to the DUV region. Thus, one can conclude that the combination of an alkali metal with borates leads to the generation of promising DUV-NLO crystals. This work is aimed at qualitative and quantitative investigation to report a reliable SHG value and provide details of the NLO tensor for bulk  $\text{Li}_3\text{B}_5\text{O}_8(\text{OH})_2$  single crystals.

Received 3rd September 2017,  
Accepted 30th October 2017

DOI: 10.1039/c7cp06006h

rsc.li/pccp

## 1. Introduction

The second harmonic generation (SHG) phenomenon is of great interest and has attracted tremendous attention in laser science and technology.<sup>1</sup> Nonlinear optical (NLO) crystals are widely used in optical frequency conversion<sup>2–7</sup> and produce laser radiation at wavelengths that are inaccessible *via* conventional sources.<sup>8–11</sup> In order to produce laser radiation in the ultraviolet (UV) and deep-ultraviolet (DUV) regions, a wide energy band gap is very essential. Therefore, the crystal should exhibit a short absorption cutoff and relatively high birefringence, and the refractive indices dispersion in the UV and DUV regions must be small enough to match the fundamental wave with SHG light.<sup>12</sup> Thus, the designing of efficient and high-performing NLO crystals remains challenging. Borate NLO

crystals are among the most promising candidates for this job.<sup>13,14</sup> In borate NLO crystals, B and O atoms form planar triangles ( $\text{BO}_3$ )<sup>3–</sup> and ( $\text{BO}_4$ )<sup>5–</sup> polyhedra. The  $\text{BO}_3$  groups can adopt a coplanar configuration promoting birefringence and SHG. In  $\text{BO}_3$  groups, three O atoms are linked with a B atom, eliminating three dangling bonds of the  $\text{BO}_3$  groups, which further widens its transparency in the UV and DUV region. Moreover, the highly anisotropic electron distribution in the  $\text{BO}_3$  group favors the NLO properties and birefringence,<sup>15</sup> and the large electro-negativity difference between B and O atoms is very favorable for transmittance of short-wavelength light.<sup>16</sup>  $\text{KBe}_2\text{BO}_3\text{F}_2$  (KBBF) and  $\text{Sr}_2\text{Be}_2\text{B}_2\text{O}_7$  (SBBO) single crystals<sup>17–19</sup> are very good and promising NLO crystals for generating SHG in the DUV region but due to the high toxicity of the beryllium oxide powders, it remains challenging to safely grow crystals of large size. Therefore, searching for safely grown novel NLO crystals which are able to produce coherent radiation in the UV and DUV regions has attracted the attention of many researchers. Recently, Yang *et al.*<sup>15</sup> substituted Be by Zn to eliminate the toxicity components inherent in the synthesis of KBBF and SBBO from the beryllium oxide powder. Therefore, the

New Technologies - Research Centre, University of West Bohemia, Univerzitni 8, 306 14 Pilsen, Czech Republic. E-mail: maalidph@yahoo.co.uk; Fax: +420-386 361255; Tel: +420 777729583

† Electronic supplementary information (ESI) available. See DOI: 10.1039/c7cp06006h

1 discovery of new crystals opens the way to safe crystal growth  
and increases the efficiency of the SHG to almost double in  
borate crystals due to the presence of the distorted  $(\text{ZnO}_4)^{6-}$   
tetrahedra. Moreover, the introduction of Zn atoms causes a  
5 red-shift of the  $\text{CsZn}_2\text{B}_3\text{O}_7$  absorption edge to 218 nm.<sup>15</sup> We  
should emphasize that the unique photochemistry of the  
borate non-centro-symmetric crystals may be utilized to launch  
some new photoreaction pathways. Lithium borates have  
attracted significant interest due to their outstanding proper-  
10 ties and structural diversity, and the latter is very impressive  
due to the fact that boron coordinates with three or four oxygen  
atoms forming a  $\text{BO}_3$  triangle or a  $\text{BO}_4$  tetrahedron. The  $\text{BO}_3$   
triangle or  $\text{BO}_4$  unit defines the structure of the borate. Because  
of the  $[\text{BO}_3]$  and  $[\text{BO}_4]$  units, borate crystals are often found to  
15 possess hybridized electronic band structures. Lithium borates  
exhibit piezoelectricity performance,<sup>20</sup> a strong NLO effect<sup>21</sup>  
and fast ionic conduction.<sup>22</sup> We should emphasize that the  
presence of lithium in the borate crystals ( $\text{Li}_3\text{B}_5\text{O}_8(\text{OH})_2$ ) makes  
these crystals efficient NLO crystals in the UV and DUV regions  
20 which is attributed to the fact that the alkali-metals do not have  
the d–d or f–f electronic transitions in the closed d or f orbitals  
which have an adverse influence on the band gap value. It has  
been reported that the polar Li-borates, for instance,  
 $\text{Li}_3\text{B}_5\text{O}_8(\text{OH})_2$  or  $\text{Li}_2\text{B}_4\text{O}_7$ <sup>23,24</sup> are promising materials for non-  
25 linear optical, acoustic, and thermo luminescence  
applications.<sup>25</sup> Such promising properties have motivated  
researchers to search for novel acentric or polar compounds  
in borates with lithium atoms, which are relatively rare.

Due to the excellent properties of alkaline metal borates, the  
30 combination of the alkaline metal with borate is expected to  
produce a new class of novel NLO crystals. Also, it has been  
reported that the combinations of the alkaline metal borates  
with wide transparency are prospective materials for efficient  
NLO properties. It is well known that alkaline metal borates  
35 have a perovskite-like structure. The compounds with a  
perovskite-like structure display interesting structure–property  
relationships. It has been reported that the introduction of  
alkali metal atoms can widen the transparency of borates in the  
ultra-violet region.<sup>26–29</sup> Thus the incorporation of the alkali  
40 cations into the borate system could lead to interesting and  
novel properties. As  $\text{Li}_3\text{B}_5\text{O}_8(\text{OH})_2$  crystals possess a perovskite-  
related structure, it is expected that they exhibit wide transpar-  
ency which makes them promising candidates for ultra-violet  
absorption edge materials. These unique properties can make  
45  $\text{Li}_3\text{B}_5\text{O}_8(\text{OH})_2$  ideal NLO crystals. It has been reported that  
 $\text{Li}_3\text{B}_5\text{O}_8(\text{OH})_2$  crystals display some very unusual growth  
features that are absent in many other alkali borates.<sup>30</sup>

Therefore, based on previous experimental work on the  
50 synthesis of  $\text{Li}_3\text{B}_5\text{O}_8(\text{OH})_2$  single crystals, we use this advantage  
to investigate the sources of large linear and nonlinear optical  
properties in  $\text{Li}_3\text{B}_5\text{O}_8(\text{OH})_2$  single crystals taking into account  
the influence of the packing of structural units. It is important  
to mention that, on the basis of anionic group theory,<sup>31</sup> the  
55 overall SHG response of a crystal is the geometrical super-  
position of the second-order susceptibilities. Therefore, the  
packing of the  $\text{BO}_3$  structural unit may also affect the

macroscopic SHG coefficients.<sup>32</sup> The large SHG is due to  
hyperpolarizability formed by the cations and co-parallel  $\text{BO}_3$   
triangle groups.<sup>32</sup> Therefore, this work is aimed at qualitative  
and quantitative investigation to report reliable SHG values and  
5 the details of the NLO tensor for  $\text{Li}_3\text{B}_5\text{O}_8(\text{OH})_2$  single crystals.

## 2. Materials and method

### 2.1. Methodology

10 In order to gain insight into the microscopic mechanism of the  
linear and nonlinear optical properties of  $\text{Li}_3\text{B}_5\text{O}_8(\text{OH})_2$  single  
crystals, we performed first-principles calculations using the  
full-potential method. To perform accurate calculations, the  
experimental crystallographic data of lithium borate  
15  $\text{Li}_3\text{B}_5\text{O}_8(\text{OH})_2$ <sup>23,25,30</sup> are optimized utilizing the all-electron  
full-potential method (wien2k code<sup>33</sup>) within the Perdew-  
Burke–Ernzerhof generalized gradient approximation (PBE-  
GGA).<sup>34</sup> The resulting optimized geometrical structure is used  
to calculate the ground state properties using the recently  
20 modified Becke–Johnson potential (mBJ).<sup>35</sup> The crystal struc-  
ture of lithium borate  $\text{Li}_3\text{B}_5\text{O}_8(\text{OH})_2$  is depicted in Fig. 1. For  
the DFT calculation, the basis functions in the interstitial  
region are expanded up to  $R_{\text{MT}} \times K_{\text{max}} = 7.0$  and inside the  
atomic spheres for the wave function.  $l_{\text{max}} = 10$  and the charge  
25 density is Fourier expanded up to  $G_{\text{max}} = 12$  (a.u.)<sup>-1</sup>. To obtain  
accurate self-consistency, a mesh of 4500  $\vec{k}$  points in the  
irreducible Brillouin zone (IBZ) is used. The self-consistent  
calculations are converged since the total energy of the system  
is stable within 0.00001 Ry. A mesh of 50 000  $\vec{k}$  points in the IBZ  
30 is used to perform the calculation of the linear and NLO  
properties. The inputs required for calculating the linear and  
NLO properties are the energy eigenvalues and eigenfunctions  
which are the natural outputs of band structure calculation.  
The linear optical properties are calculated using the optical  
35 code implemented in the Wien2k package;<sup>33</sup> for more details  
we refer readers to the users' guide<sup>36</sup> and ref. 37. The formalism  
for calculating the nonlinear optical properties is given  
elsewhere.<sup>38–41</sup>

40 It is well known that the DFT approaches have the ability to  
accurately predict the ground state properties of the materials,  
and the developed analytical tools are vital to investigate their  
intrinsic mechanism. This microscopic understanding has  
further guided molecular engineering design for new crystals  
45 with novel structures and properties. It is anticipated that  
first-principles material approaches will greatly improve the  
search efficiency and greatly help experiments to save  
resources in the exploration of new crystals with good  
performance.<sup>42–51</sup> For instance, several researchers have used  
50 DFT calculations for exploration of the linear and nonlinear  
optical properties of new NLO materials and have found good  
agreement with the experimental results. We would like to  
mention here that, in our previous studies,<sup>52–55</sup> we have  
calculated the linear and nonlinear optical properties using  
55 the FPLAPW method for several systems whose linear and  
nonlinear optical susceptibility dispersions are known

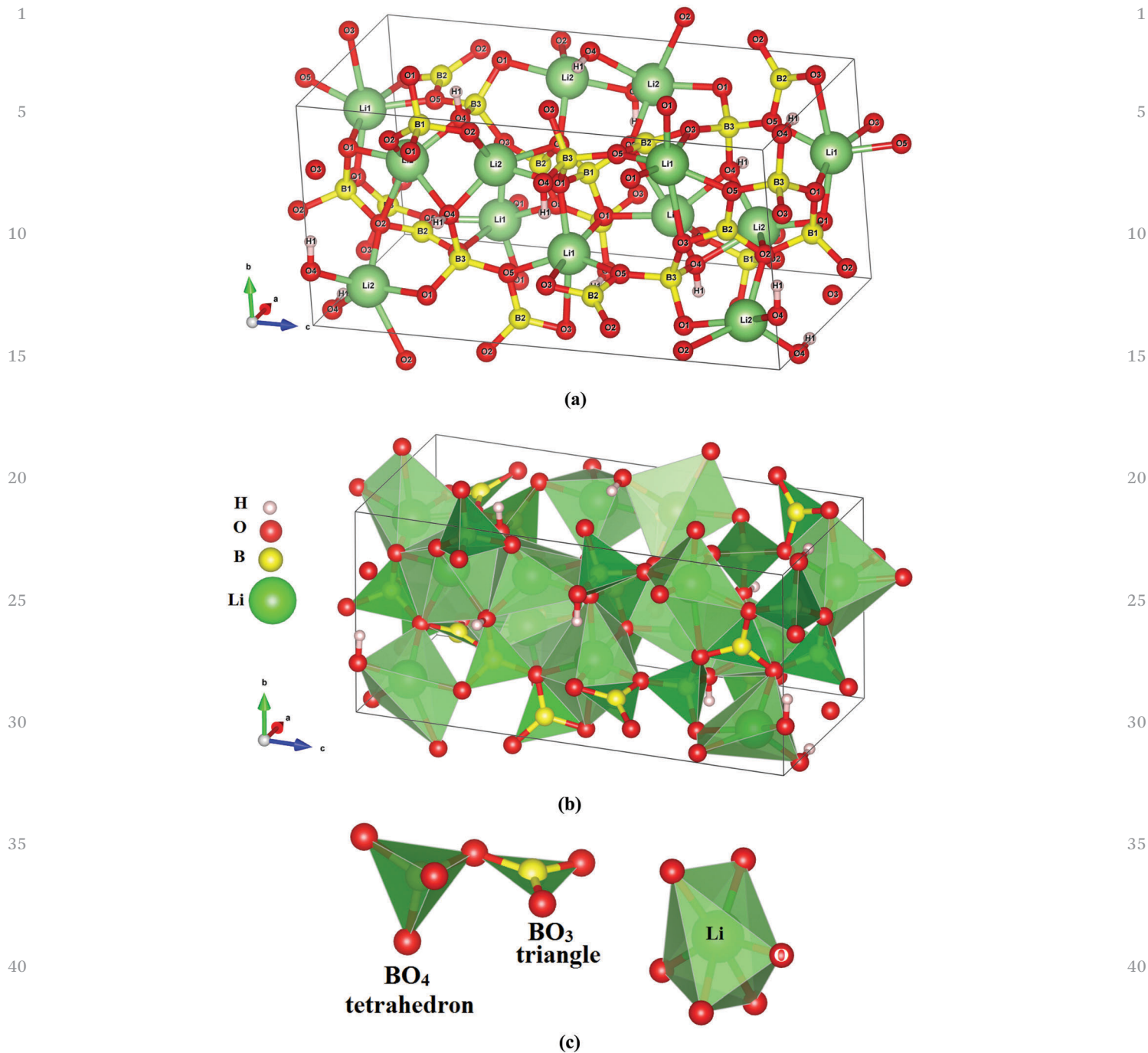


**Fig. 1** (a–c) The crystal structure of  $\text{Li}_3\text{B}_5\text{O}_8(\text{OH})_2$  which crystallizes in the noncentrosymmetric tetragonal space group  $P41212$ , No. 92 with four formula units per unit cell. The unit cell consists of two lithium, three boron and five oxygen atoms *i.e.* ten independent atoms. The crystal structure of the tetragonal lithium borate  $\text{Li}_3\text{B}_5\text{O}_8(\text{OH})_2$  consists of Li–O polyhedra and the  $[\text{B}_5\text{O}_8(\text{OH})_2]^{3-}$  polyborate anion. The  $[\text{B}_5\text{O}_8(\text{OH})_2]^{3-}$  polyborate anion consists of two 6-membered rings in which two B atoms are surrounded by three O atoms ( $\text{BO}_3$  triangle), and the other three B atoms are surrounded by four O atoms ( $\text{BO}_4$  tetrahedron). Each 6-membered ring is linked by a common  $\text{BO}_4$  tetrahedron and consists of one  $\text{BO}_3$  triangle, one  $\text{BO}_3(\text{OH})$  tetrahedron, and a common  $\text{BO}_4$  tetrahedron. The  $[\text{B}_5\text{O}_8(\text{OH})_2]^{3-}$  units are linked together through four exocyclic O atoms to neighboring units and formed a 3-D structure. Moreover, there also exist hydrogen bonds between the framework hydroxyl groups and the exocyclic O atoms. The  $\text{Li}^+$  ions are located in the anionic  $[\text{B}_5\text{O}_8(\text{OH})_2]^{3-}$  framework and compensate its negative charge. There are two kinds of coordinated forms for  $\text{Li}^+$  ions. Li1 exhibits a 5-fold coordination and coordinates to three O atoms from B–O–B bridges and two O atoms from hydroxyl groups. Li2 exhibits a 6-fold coordination and coordinates to four O atoms from B–O–B bridges and two exocyclic O atoms. The  $\text{BO}_3$  triangles adopt a nearly coplanar configuration, which enhances the SHG and the birefringence in borate crystals.

experimentally and very good agreement with the experimental data was obtained. Thus, we believed that our calculations reported in this paper would produce very accurate and reliable results.

## 2.2. Crystal structure

It has been reported that  $\text{Li}_3\text{B}_5\text{O}_8(\text{OH})_2$  crystallizes in the noncentrosymmetric tetragonal space group  $P41212$ , No. 92 with four formula units per unit cell and unit cell parameters of  $a = 6.891(4) \text{ \AA}$ ,  $c = 14.615(12) \text{ \AA}$ .<sup>23,25,30</sup> The unit cell consists of two lithium, three boron and five oxygen atoms *i.e.* ten independent atoms<sup>23,25,30</sup> (see Fig. 1). The crystal structure of the tetragonal lithium borate  $\text{Li}_3\text{B}_5\text{O}_8(\text{OH})_2$  consists of Li–O polyhedra and the  $[\text{B}_5\text{O}_8(\text{OH})_2]^{3-}$  polyborate anion. The  $[\text{B}_5\text{O}_8(\text{OH})_2]^{3-}$  polyborate anion consists of two 6-membered rings in which two B atoms are surrounded by three O atoms ( $\text{BO}_3$  triangle), and the other three B atoms are surrounded by four O atoms ( $\text{BO}_4$  tetrahedron). Each 6-membered ring is linked by a common  $\text{BO}_4$  tetrahedron and consists of one  $\text{BO}_3$  triangle, one  $\text{BO}_3(\text{OH})$  tetrahedron, and a common  $\text{BO}_4$  tetrahedron. The  $[\text{B}_5\text{O}_8(\text{OH})_2]^{3-}$  units are linked together through four exocyclic O atoms to neighboring units and formed a 3-D structure. Moreover, there also exist hydrogen

bonds between the framework hydroxyl groups and the exocyclic O atoms. The  $\text{Li}^+$  ions are located in the anionic  $[\text{B}_5\text{O}_8(\text{OH})_2]^{3-}$  framework and compensate its negative charge. There are two kinds of coordinated forms for  $\text{Li}^+$  ions. Li1 exhibits a 5-fold coordination and coordinates to three O atoms from B–O–B bridges and two O atoms from hydroxyl groups. Li2 exhibits a 6-fold coordination and coordinates to four O atoms from B–O–B bridges and two exocyclic O atoms.

The experimental crystallographic data<sup>23,25,30</sup> were used as input to perform geometrical relaxation. The experimental lattice parameters were optimized and the experimental atomic positions were relaxed by minimizing the forces acting on each atom; we assume that the structure is totally relaxed when the forces on each atom reach values less than 1 mRy/a.u. The relaxed geometry of  $\text{Li}_3\text{B}_5\text{O}_8(\text{OH})_2$  is provided in the ESI.† Geometrical relaxation was achieved by using PBE-GGA. From the relaxed geometry, the electronic band structure was obtained using mBJ. We should emphasize that the mBJ

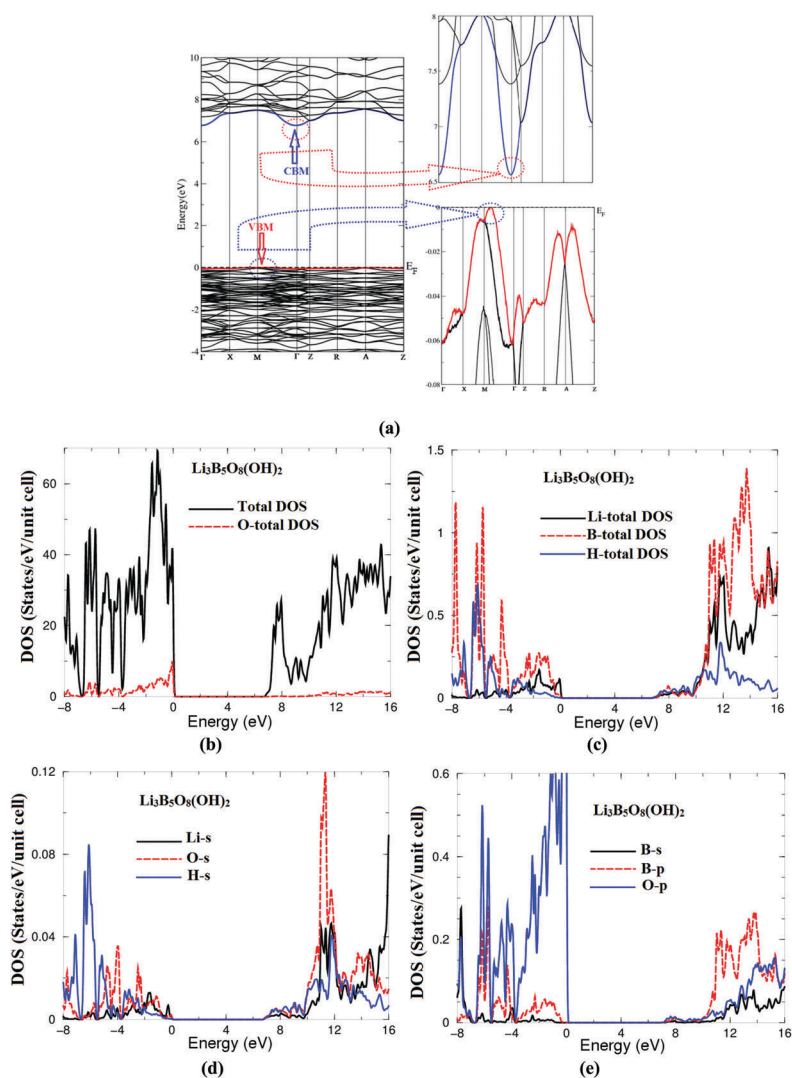


Fig. 2 (a) Calculated electronic band structure of  $\text{Li}_3\text{B}_5\text{O}_8(\text{OH})_2$  along with the enlarged bands around the Fermi level *i.e.* the VBM and the CBM; (b–e) the calculated angular momentum projected density of states of  $\text{Li}_3\text{B}_5\text{O}_8(\text{OH})_2$ .

1 succeeds by a large amount in bringing the calculated energy  
 2 gap closer to the experimental one. Therefore, the results  
 3 obtained by mBJ are shown below. Based on the calculated  
 4 band structure, the complex first-order linear and second-order  
 5 non-linear optical dispersions are obtained.

### 3. Obtained results and discussion

10 The obtained electronic band structure of the tetragonal  
 11  $\text{Li}_3\text{B}_5\text{O}_8(\text{OH})_2$  crystals reveals the nature of the band gap and  
 12 the high  $k$ -dispersion bands around the Fermi level ( $E_F$ ) as  
 13 shown in Fig. 2a. One can see that the top of the valence band  
 14 (VBM) is located at the  $M$  point of the first BZ whereas the  
 15 bottom of the conduction band (CBM) is situated at  $\Gamma$  resulting  
 16 in a direct band gap. The calculated energy band gap's value  
 17 using mBJ is estimated to be 6.52 eV in close agreement with  
 18 the experimental values (6.526 eV).<sup>23,25,30</sup> Therefore, a material  
 19 with such an energy band gap value is expected to possess a  
 20 high laser damage threshold.<sup>56,57</sup> It is necessary to highlight  
 21 that the high  $k$ -dispersion bands around  $E_F$  possess low effective  
 22 masses and, hence, high mobility carriers, which enhances  
 23 the charge transfer process. The mobility of the photogenerated  
 24 carriers significantly influences the SHG efficiency. Moreover,  
 25 the great effective mass difference (see Table 1) between the  
 26 electron ( $e^-$ ) and the hole ( $h^+$ ) can facilitate the  $e^-$  and  $h^+$   
 27 migration and separation, and finally improve the SHG  
 28 performance.

29 To better understand the relationship between electronic  
 30 structures and optical properties, the total and the angular  
 31 momentum projected density of states (PDOS) are computed as  
 32 shown in Fig. 2b–e. This will help in gaining a detailed  
 33 description about the orbitals that form the VBM and the  
 34 CBM and the orbitals which are responsible for the optical  
 35 transitions according to the dipole selection rules. The  
 36 obtained PDOS helps in identifying the angular momentum  
 37 character of the various structures. It was found that the VBM  
 38 originates mainly from O-2p states with small contribution  
 39 from Li-2s and O-2s states whereas the CBM is formed by O-  
 40 2p and B-2p states with small contributions from H-1s, O-2s  
 41 and Li-2s states. Furthermore, a strong hybridization between  
 42 Li-2s, O-2s and Li-2s is observed, and also O-2-p states form  
 43 strong hybridization with B-2s/2p states. The hybridization  
 44 favors the enhancement of the covalent bonding, and hence,  
 45 the optical performance due to the fact that covalent bonding is  
 46 more favorable for the transport of the carriers than the ionic  
 47 one.<sup>58</sup>

48 In order to elucidate the characteristics of chemical bonding  
 49 of  $\text{Li}_3\text{B}_5\text{O}_8(\text{OH})_2$ , the calculated angular momentum projected  
 50 density of states was used (Fig. 2b–e). The structure of the  
 51 valence bands that is confined between  $-8.0$  eV and  $E_F$  is

mainly formed by O-2s/2p, H-1s, Li-2s and B-2s/2p orbitals.  
 The total number of electrons/electron volts (e/eV) of these  
 orbitals was obtained as follows; O-2p orbital 0.7 e/eV, B-2p  
 orbital 0.28 e/eV, B-2s orbital 0.28 e/eV, Li-2s orbital 0.016 e/eV,  
 O-2s orbital 0.038 e/eV and H-1s orbital 0.082 e/eV. One can  
 conclude that some electrons from O-2s/2p, H-1s, Li-2s and B-  
 2s/2p orbitals were transferred to the VBs and participated in  
 the interactions between the atoms to form covalent bonding.  
 The strength of the covalent bond depends on the degree of  
 hybridization and electro-negativity differences between the  
 atoms. This can be seen directly from the contours of the  
 valence electronic charge density of each atom in  $\text{Li}_3\text{B}_5\text{O}_8(\text{OH})_2$ .  
 These contours were obtained in different crystallographic  
 planes as shown in Fig. 3. Fig. 3a, shows the (1 0 0) crystal-  
 10 lographic plane; it can be seen that the B atom forms strong  
 11 covalent bonds with the nearest O atoms in  $\text{BO}_3$  and  $\text{BO}_4$  (see  
 12 Fig. 3b–d). Due to the electro-negativity differences between B  
 13 (2.04) and O (3.44) charge transfer occurs towards O atoms as  
 14 they are surrounded by uniform spheres. It was reported that in  
 15 borate materials, the large electro-negativity difference between  
 16 B and O atoms is very favorable for transmittance of short-  
 17 wavelength light.<sup>59</sup> In general, the B and O atoms in borates  
 18 form planar triangles ( $\text{BO}_3$ )<sup>3-</sup> and ( $\text{BO}_4$ )<sup>5-</sup> polyhedra. The  $\text{BO}_3$   
 19 groups can adopt a coplanar configuration promoting birefrin-  
 20 gence and SHG. In  $\text{BO}_3$  groups, three O atoms are linked with  
 21 the B atom, eliminating three dangling bonds of the  $\text{BO}_3$   
 22 groups, which further widens its transparency in the UV and  
 23 DUV region. Moreover, the high anisotropic electron distribu-  
 24 tion in the  $\text{BO}_3$  group favors the enhancement of the SHG and  
 25 birefringence.<sup>60</sup> More details can be seen from the (1 0 1)  
 26 crystallographic plane (Fig. 3b), which reveals that the Li atoms  
 27 form ionic bonding. Also it shows the ( $\text{BO}_3$ )<sup>3-</sup> triangles and  
 28 ( $\text{BO}_4$ )<sup>5-</sup> polyhedra. This supports the finding from the PDOS,  
 29 which states that there exists strong hybridization between B  
 30 and O atoms. The strong/weak hybridization may lead to the  
 31 formation of strong/weak covalent bonding. It is interesting to  
 32 compare our calculated bond lengths with the measured  
 33 ones,<sup>23,25,30</sup> as shown in Table 2, which reveals that there is  
 34 good agreement between the theory and the experiment.

35 To confirm that the absorption edge of the tetragonal  
 36  $\text{Li}_3\text{B}_5\text{O}_8(\text{OH})_2$  occurs in the DUV region, the absorption spectra  
 37 are calculated, as presented in Fig. 4a. The absorption edge's  
 38 value of the semiconductor materials could be solved as  
 39 follows; the square of the absorption coefficient  $I(\omega)$  is linear  
 40 with energy ( $E$ ) for direct optical transitions in the absorption  
 41 edge region, whereas the square root of  $I(\omega)$  is linear with  $E$  for  
 42 indirect optical transitions.<sup>61,62</sup> The data plots of  $\text{SQRT}[I(\omega)]$   
 43 and  $\text{SQ}[I(\omega)]$  versus  $E$  in the absorption edge region are shown  
 44 in Fig. 4b and c. The left inset of Fig. 4b shows that the  
 45  $\text{SQRT}[I(\omega)]$  vs. energy deviates from the fitted straight line,  
 46 whereas  $\text{SQ}[I(\omega)]$  vs.  $E$  is nearly linear (Fig. 4c). These features  
 47 suggest that the absorption edge of  $\text{Li}_3\text{B}_5\text{O}_8(\text{OH})_2$  caused by  
 48 direct transitions and the charge transfer from the O-2p orbital  
 49 at the VBM to the B-2p orbital at the CBM contributes to the  
 50 absorption edge. Thus, the optical properties of  $\text{Li}_3\text{B}_5\text{O}_8(\text{OH})_2$   
 51 arise due to the transitions between B-2p and O-2p orbitals with

Table 1 Calculated effective masses

$m_e^*/m_0$	$m_h^*/m_0$	$D = m_e^*/m_h^*$	$D = m_h^*/m_e^*$
0.01202	0.01988	0.60462	1.65391



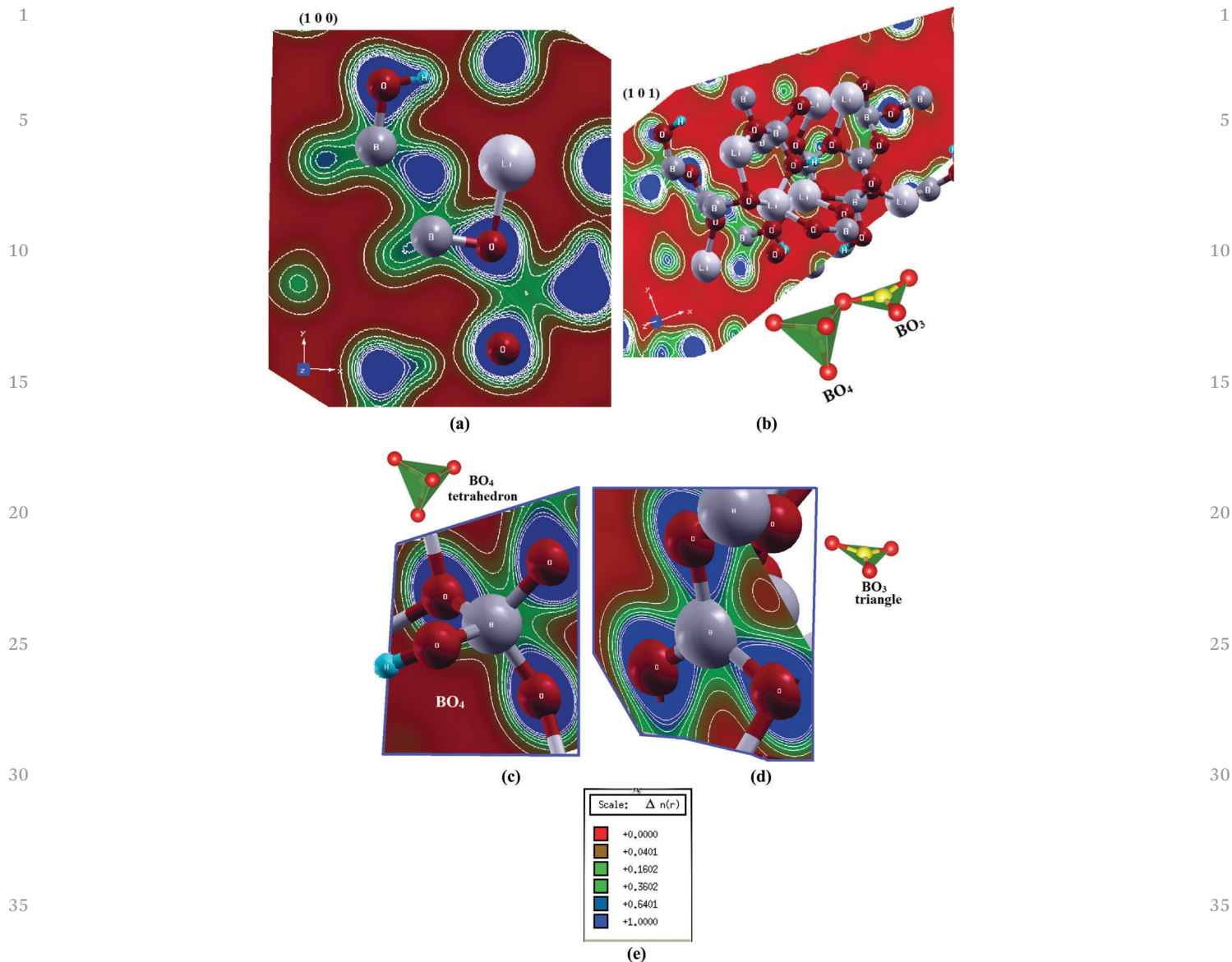


**Fig. 3** (a and b) The electron cloud of  $\text{Li}_3\text{B}_5\text{O}_8(\text{OH})_2$  in two crystallographic planes namely (100) and (101); (c and d) the electron cloud of the  $\text{BO}_3$  anionic groups which exhibit a planar shape with conjugated electron orbitals which make the  $\text{BO}_3$  anionic groups the main source of the large birefringence in  $\text{Li}_3\text{B}_5\text{O}_8(\text{OH})_2$ . The electron cloud of the  $\text{BO}_4$  tetrahedron; (e) thermo-scale.

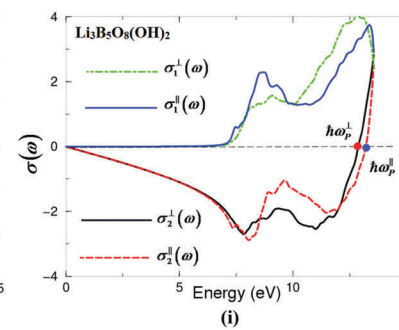
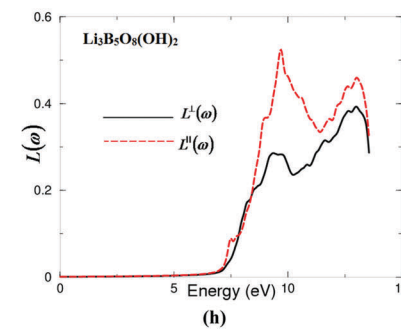
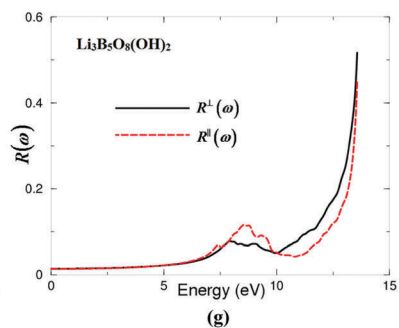
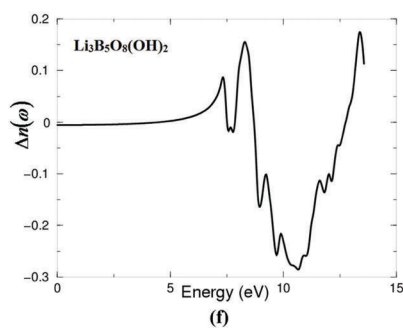
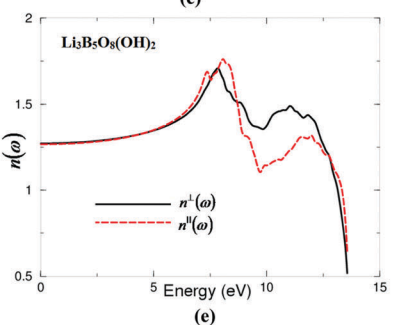
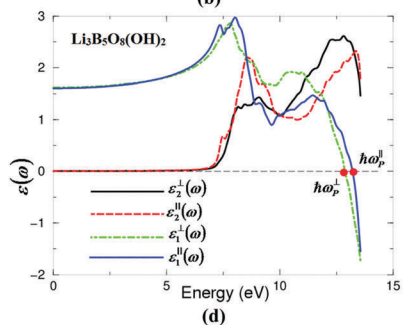
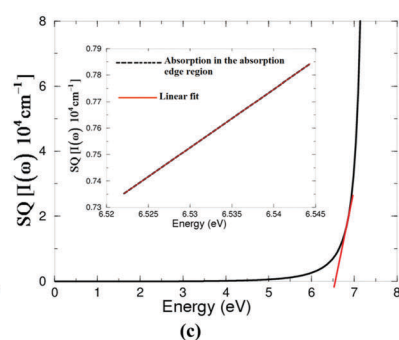
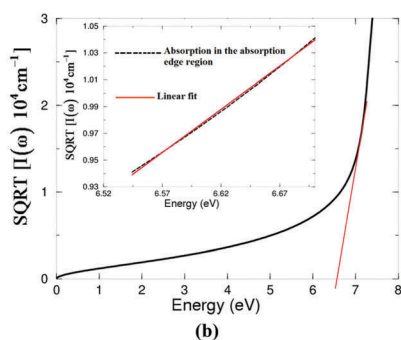
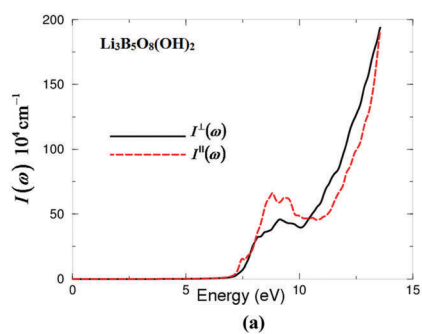
**Table 2** Calculated bond lengths in comparison with the experimental data<sup>25b</sup>

Bond	Exp. bond lengths (Å)	Calc. bond lengths (Å)
Li(1)–O(5)	1.962(3)	1.960
Li(1)–O(3)	2.009(3)	2.002
Li(1)–O(2)	2.035(3)	2.033
Li(2)–O(1)	2.0242(15)	2.0239
Li(2)–O(2)	2.056(3)	2.054
Li(2)–O(4)	2.436(3)	2.434
B(1)–O(3)	1.3765(18)	1.3760
B(2)–O(1)	1.4772(18)	1.4769
B(3)–O(2)	1.4636(15)	1.4632
B(3)–O(3)	1.4964(16)	1.4960

small contributions from Li-2s and H-1s orbitals. Following Fig. 4c, we can conclude that the absorption edge of

$\text{Li}_3\text{B}_5\text{O}_8(\text{OH})_2$  occurs at  $\lambda = 190$  nm and the optical band gap is estimated to be 6.52 eV in good agreement with the experimental data (6.526 eV).<sup>23,25,30</sup>

This observation motivated us to demonstrate the calculated imaginary and real parts of the optical dielectric function (Fig. 4d). The imaginary part shows the first critical points (the absorption edges) for the perpendicular and parallel tensor components along the fundamental crystal axes, which are located at 6.52 eV and the fundamental peaks situated at 8.5 and 12.5 eV. Furthermore, the imaginary part reveals that  $\epsilon_2^{\parallel}(\omega)$  is the dominant tensor component at low energies while  $\epsilon_2^{\perp}(\omega)$  acts as the dominant tensor component at high energies, resulting in a considerable anisotropy. The calculated vanishing frequency value (static electronic dielectric constant



1 **Fig. 4** (a) The calculated absorption spectra of  $\text{Li}_3\text{B}_5\text{O}_8(\text{OH})_2$ ; (b and c) the data plots of  $\text{SQRT}[\epsilon(\omega)]$  and  $\text{SQ}[\epsilon(\omega)]$  versus  $E$  in the absorption edge region  
 1 are shown in (b) and (c). The left inset of (b) shows that the  $\text{SQRT}[\epsilon(\omega)]$  vs. energy deviates from the fitted straight line, whereas  $\text{SQ}[\epsilon(\omega)]$  vs.  $E$  is nearly linear.  
 2 These features suggest that the absorption edge of  $\text{Li}_3\text{B}_5\text{O}_8(\text{OH})_2$  caused by indirect transitions and the charge transfer from the O-2p orbital at the VBM  
 3 to the B-2p orbital at the CBM contributes to the absorption edge. Thus, the optical properties of  $\text{Li}_3\text{B}_5\text{O}_8(\text{OH})_2$  arise due to the transitions between B-2p  
 4 and O-2p orbitals with small contributions from Li-2s and H-1s orbitals. We can conclude that the absorption edge of  $\text{Li}_3\text{B}_5\text{O}_8(\text{OH})_2$  occurs at  $\lambda = 190$  nm  
 5 and the optical band gap is estimated to be 6.52 eV in good agreement with the experimental data (6.526 eV); (d) calculated  $\epsilon_2^\perp(\omega)$  (dark solid curve-black  
 6 color online) and  $\epsilon_2^\parallel(\omega)$  (light dashed curve-red color online) along with calculated  $\epsilon_1^\perp(\omega)$  (light dotted dashed curve-green color online) and  $\epsilon_1^\parallel(\omega)$  (light  
 7 dotted curve-blue color online); (e) calculated  $n^\perp(\omega)$  (dark solid curve-black color online) and  $n^\parallel(\omega)$  (light dashed curve-red color online); (f) calculated  
 8 birefringence  $\Delta n(\omega)$ ; (g) calculated  $R^\perp(\omega)$  (dark solid curve-black color online) and  $R^\parallel(\omega)$  (light dashed curve-red color online); (h) calculated  $L^\perp(\omega)$  (dark  
 9 solid curve-black color online) and  $L^\parallel(\omega)$  (light dashed curve-red color online); (i) calculated  $\sigma_2^\perp(\omega)$  (dark solid curve-black color online) and  $\sigma_2^\parallel(\omega)$  (light  
 10 dashed curve-red color online) along with calculated  $\sigma_1^\perp(\omega)$  (light dotted dashed curve-green color online) and  $\sigma_1^\parallel(\omega)$  (light dotted curve-blue color  
 11 online).

12  $\epsilon_\infty = \epsilon_1^\perp(0)$  and  $\epsilon_\infty = \epsilon_1^\parallel(0)$  of  $\epsilon_1^\perp(\omega)$  and  $\epsilon_1^\parallel(\omega)$  confirms the  
 13 occurrence of absorption edges at 6.52 eV, which can be  
 14 explained on the basis of the Penn model  $\epsilon_1(0) \approx 1 +$   
 15  $(\hbar\omega_p/E_{\text{optical gap}})^{2,63}$  where the calculated  $\epsilon_1(0)$  is inversely  
 16 related to the energy gap. For  $\text{Li}_3\text{B}_5\text{O}_8(\text{OH})_2$  the calculated  
 17  $\epsilon_1(0)$  and the plasma energy  $\hbar\omega_p$  are given in Table 3. Thus,  
 18 the  $E_{\text{optical gap}}$  is about 6.52 eV and  $\lambda = 1239.8/E_{\text{optical gap}} = 190$  nm.  
 19 Therefore, the calculated  $\epsilon_2^\perp(\omega)$ ,  $\epsilon_2^\parallel(\omega)$ ,  $\epsilon_1^\perp(\omega)$ ,  $\epsilon_1^\parallel(\omega)$ ,  $\epsilon_1^\perp(0)$  and  
 20  $\epsilon_1^\parallel(0)$  support our observation that the absorption edge of  
 21  $\text{Li}_3\text{B}_5\text{O}_8(\text{OH})_2$  occurs at  $\lambda = 190$  nm and the optical band gap is  
 22 estimated to be 6.52 eV in good agreement with the experimental  
 23 data (6.526 eV).<sup>23,25,30</sup> Furthermore, the calculated values  
 24 of  $\epsilon_1^\perp(0)$  and  $\epsilon_1^\parallel(0)$  help in estimating a very important quantity  
 25 which is called uniaxial anisotropy using the relation  $\delta_e =$   
 26  $[(\epsilon_0^\parallel - \epsilon_0^\perp)/\epsilon_0^{\text{avg}}]$ .<sup>64</sup> It is found that the uniaxial anisotropy of  
 27  $\text{Li}_3\text{B}_5\text{O}_8(\text{OH})_2$  is about  $-0.0081$ , which confirms the considerable  
 28 anisotropy. The considerable anisotropy favors an important  
 29 quantity in SHG and OPO due to better fulfilling of phase-  
 30 matching conditions determined by birefringence. The birefrin-  
 31 gence can be obtained from the calculated refractive indices  
 32 (Fig. 4e) using the expression  $\Delta n(\omega) = n_e(\omega) - n_o(\omega)$ , see Fig. 4f.  
 33 The obtained values of the birefringence at the static limit,  $\lambda =$   
 34  $1064$  nm and at  $\lambda = 190$  nm are given in Table 3. Birefringence is  
 35 important in fulfilling the phase-matching conditions. Further-  
 36 more, the calculated refractive indices (Fig. 4e) confirm the value  
 37 of  $n(0) = \sqrt{\epsilon_1(0)}$ , Fig. 4e shows that  $n^{\text{average}}(0)$  occurs at 1.27  
 38 thus  $\epsilon_1^{\text{average}}(0) = 1.61$ , and hence, the absorption edges of  
 39  $\text{Li}_3\text{B}_5\text{O}_8(\text{OH})_2$  occur at  $\lambda = 190$  nm. The calculated refractive  
 40 indices at zero limit, at  $\lambda = 190$  nm (6.52 eV) and  $\lambda = 1064$  nm are

41 **Table 3** The calculated energy band gap in comparison with the experi-  
 42 mental value,  $\epsilon_1^\perp(0)$ ,  $\epsilon_1^\parallel(0)$ ,  $\hbar\omega_p^\perp$ ,  $\hbar\omega_p^\parallel$ ,  $n^\perp(\omega)$ ,  $n^\parallel(\omega)$ ,  $\Delta n(0)$  and  $\Delta n(\omega)$

$E_g$ (eV)	6.52, 6.526 <sup>a</sup>
$\epsilon_1^\perp(0)$	1.619
$\epsilon_1^\parallel(0)$	1.606
$\delta_e$	-0.0081
$\hbar\omega_p^\perp$	12.884
$\hbar\omega_p^\parallel$	13.211
$n^\perp(\omega)$	1.272 <sup>b</sup> , 1.275 <sup>c</sup> , 1.450 <sup>d</sup> ,
$n^\parallel(\omega)$	1.267 <sup>b</sup> , 1.270 <sup>c</sup> , 1.473 <sup>d</sup> ,
$\Delta n(\omega)$	-0.005 <sup>b</sup> , -0.006 <sup>c</sup> , +0.0141 <sup>d</sup>

43 <sup>a</sup> Ref. 23, 25, 30 (experimental work). <sup>b</sup> Ref. this work at zero limit.  
 44 <sup>c</sup> Ref. this work at  $\lambda = 1064$  nm. <sup>d</sup> Ref. this work at  $\lambda = 190$  nm.

12 shown in Table 3 and they are small enough to match the  
 13 fundamental wave with the SHG light.

14 To further investigate the linear optical susceptibility dis-  
 15 persion, the reflectivity spectra and the loss function are  
 16 calculated. The reflectivity spectra (Fig. 4g) show the first  
 17 minimum at the plasma frequency (*i.e.* 12.5 eV), the energy  
 18 point where optical spectra of  $\epsilon_1^\perp(\omega)$  and  $\epsilon_1^\parallel(\omega)$  cross zero,  
 19 confirming the occurrence of collective plasmon resonance in  
 20 concordance with our observation in Fig. 4d.

21 The loss function's peaks (Fig. 4h) are initiated at the values  
 22 of the plasma frequencies  $\omega_p^\perp$  and  $\omega_p^\parallel$  at the energy point where  
 23 optical spectra of  $\epsilon_1^\perp(\omega)$  and  $\epsilon_1^\parallel(\omega)$  cross zero. The frequency-  
 24 dependent optical conductivity (Fig. 4i) can be obtained from  
 25 the complex first-order linear optical dielectric function follow-  
 26 ing the expression  $\epsilon(\omega) = \epsilon_1(\omega) + i\epsilon_2(\omega) = 1 + \frac{4\pi i\sigma(\omega)}{\omega}$ .<sup>65,66</sup> It  
 27 consists of imaginary and real parts; therefore, it completely  
 28 characterizes the linear optical properties. The imaginary part  
 29  $\sigma_2^\perp(\omega)$  and  $\sigma_2^\parallel(\omega)$  between 0.0 and the values of  $\omega_p^\perp$  and  $\omega_p^\parallel$   
 30 exhibit overturned features of  $\epsilon_2^\perp(\omega)$  and  $\epsilon_2^\parallel(\omega)$ , whereas the real  
 31 parts  $\sigma_1^\perp(\omega)$  and  $\sigma_1^\parallel(\omega)$  show similar features to those of  $\epsilon_2^\perp(\omega)$   
 32 and  $\epsilon_2^\parallel(\omega)$ . The intersection of the imaginary and real parts of  
 33 the optical conductivity at zero energy represents the values of  
 34  $\sigma_2^\perp(\omega)$  and  $\sigma_2^\parallel(\omega)$ .

35 It has been reported that in most borate crystals the SHG  
 36 responses mainly arise from the coparallel  $\text{BO}_3$  triangles, for  
 37 instance: the KBBF derivatives contain two types of B-O groups  
 38 and one of the B-O groups consists of coparallel  $\text{BO}_3$  triangles.  
 39 The second B-O group is located between the two adjacent  
 40  $[\text{Be}_2\text{BO}_3\text{O}_2]$  and connects them together with antiparallel  
 41 arrangement, resulting in canceling their contribution to the  
 42 macroscopic SHG response. Hence, the SHG responses in KBBF  
 43 derivatives mainly arise from the coparallel  $\text{BO}_3$  triangles.  
 44 Therefore, the number density of the coparallel  $\text{BO}_3$  triangles  
 45 will determine the SHG response of the KBBF structures.<sup>53,67</sup>  
 46 Also in  $\text{CsZn}_2\text{B}_3\text{O}_7$ , the  $\text{B}_3\text{O}_6$  groups are located between  
 47 adjacent  $[\text{Zn}_2\text{BO}_3\text{O}_2]$  layers and they are antialigned. Thus,  
 48 the SHG response of  $\text{CsZn}_2\text{B}_3\text{O}_7$  should also come from the  
 49 coparallel  $\text{BO}_3$  triangles, which was confirmed by Yu *et al.*<sup>17</sup>  
 50 They reported that the net dipole moments of the  $\text{BO}_3$  triangles  
 51 and  $(\text{ZnO}_4)^{6-}$  tetrahedra are pointed along the polar  $c$ -axis  
 52 which means that  $\text{BO}_3$  triangles and  $(\text{ZnO}_4)^{6-}$  tetrahedra con-  
 53 tributions to the SHG response are larger than that of  $\text{B}_3\text{O}_6$

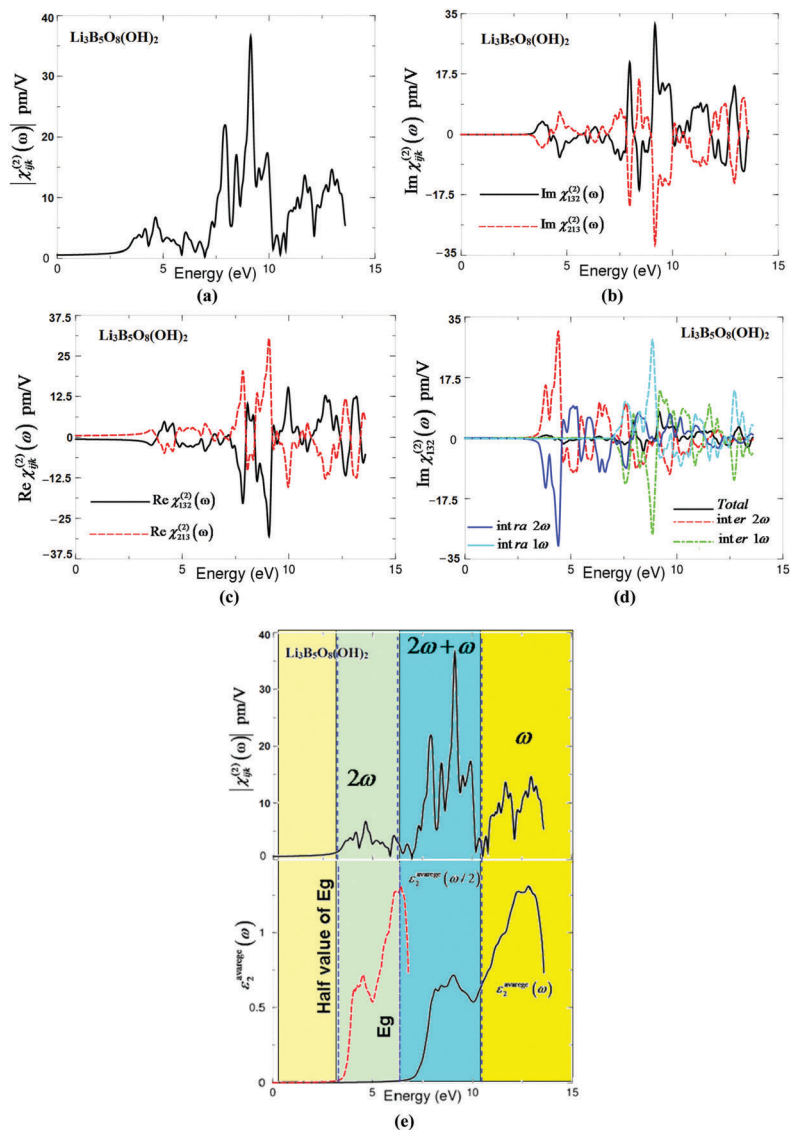


**Fig. 5** (a) Calculated  $|\chi_{ijk}^{(2)}(\omega)|$  for the five tensor components of  $\text{Li}_3\text{B}_5\text{O}_8(\text{OH})_2$ ; (b) calculated imaginary  $\chi_{132}^{(2)}(\omega)$  (dark solid curve-black color online) and  $\chi_{213}^{(2)}(\omega)$  (light dashed curve-red color online) spectra; (c) calculated real  $\chi_{132}^{(2)}(\omega)$  (dark solid curve-black color online) and  $\chi_{213}^{(2)}(\omega)$  (light dashed curve-red color online) spectra; (d) calculated total  $\text{Im}\chi_{ijk}^{(2)}(\omega)$  spectrum (dark solid curve-black color online) along with the intra ( $2\omega$ )/( $1\omega$ ) (light solid curve-blue color online)/light dashed dotted curve-cyan color online) and inter ( $2\omega$ )/( $1\omega$ ) (light long dashed curve-red color online)/light dotted curve-green color online) -band contributions; (e) upper panel: calculated  $|\chi_{ijk}^{(2)}(\omega)|$  (dark solid curve-black color online); lower panel: calculated  $\epsilon_2^{xx}(\omega)$  (dark solid curve-black color online); calculated  $\epsilon_2^{xx}(\omega/2)$  (dark dashed curve-red color online).

**Table 4** Calculated  $|\chi_{ijk}^{(2)}(\omega)|$  and  $\beta_{ijk}$   $\text{Li}_3\text{B}_5\text{O}_8(\text{OH})_2$ , in pm/V at the static limit, at  $\lambda = 190$  nm and at  $\lambda = 1064$  nm

Tensor components	$\chi_{ijk}^{(2)}(0)$	Theory $d_{ijk} = 0.5$ at static limit	$\chi_{ijk}^{(2)}(\omega)$ at $\lambda = 1064$ nm	Theory $d_{ijk} = 0.5$ $\chi_{ijk}^{(2)}(\omega)$ at $\lambda = 1064$ nm	$\chi_{ijk}^{(2)}(\omega)$ at $\lambda = 190$ nm	Theory $d_{ijk} = 0.5$ $\chi_{ijk}^{(2)}(\omega)$ at $\lambda = 190$ nm
$ \chi_{132}^{(2)}(\omega)  =  \chi_{213}^{(2)}(\omega) $	0.7	$d_{14} = 0.35$	1.28	$d_{14} = 0.64$	3.00	$d_{14} = 1.5$
$\beta_{333}$	$0.413 \times 10^{-30}$ esu	$0.206 \times 10^{-30}$ esu	$0.477 \times 10^{-30}$ esu	$0.238 \times 10^{-30}$ esu	$2.274 \times 10^{-30}$ esu	$1.137 \times 10^{-30}$ esu

groups.<sup>17</sup> Thus, based on these results and similar to other borates the SHG responses in  $\text{Li}_3\text{B}_5\text{O}_8(\text{OH})_2$  mainly arise from the coparallel  $\text{BO}_3$  triangles. Therefore, the number density of the coparallel  $\text{BO}_3$  triangles will determine the SHG response of the  $\text{Li}_3\text{B}_5\text{O}_8(\text{OH})_2$  structure. Our investigation confirms that

$\text{Li}_3\text{B}_5\text{O}_8(\text{OH})_2$  possesses large birefringence and considerable anisotropy in the linear optical properties, and the absorption edge occurs at  $\lambda = 190$  nm. Therefore, based on these promising results, we calculated the nonlinear optical susceptibility dispersion of  $\text{Li}_3\text{B}_5\text{O}_8(\text{OH})_2$ .

Due to the symmetry,  $\text{Li}_3\text{B}_5\text{O}_8(\text{OH})_2$  possesses two non-zero tensor components, these are  $132 = -213$ . The calculated  $|\chi_{132}^{(2)}(\omega)| = |\chi_{213}^{(2)}(\omega)|$  are shown in Fig. 5a. The calculated values of these tensor components at the static limit, at  $\lambda = 190$  nm and at  $\lambda = 1064$  nm, are presented in Table 4. The calculated value of SHG at  $\lambda = 1064$  nm is about 1.5 times that of the well known NLO crystal  $\text{KH}_2\text{PO}_4$  (KDP) at  $\lambda = 1064$  nm and 3.5 times that of KDP at  $\lambda = 190$  nm, which is transparent down to the deep-UV region. Thus, one can conclude that the combination of an alkali metal into borates leads to the generation of promising DUV NLO crystals.

Furthermore, we calculated the imaginary and real parts of  $\chi_{132}^{(2)}(\omega) = -\chi_{213}^{(2)}(\omega)$ , as shown in Fig. 5b and c. It is shown that the  $2\omega$  resonance starts oscillating at around 3.26 eV, the half value of the fundamental optical band gap. The highest intensity which is confined between 6.52 and 9.0 eV comes from the contribution of  $2\omega$  and  $\omega$ . The imaginary and real parts are further separated into  $2\omega/\omega$  inter-/intra-band contributions. Fig. 5d shows the  $2\omega/\omega$  inter-/intra-band contributions of the imaginary part of  $\chi_{132}^{(2)}(\omega)$ . It is clear that the  $2\omega/\omega$  inter-/intra-band contributions oscillate around zero and exhibit a considerable anisotropy. The sum of those contributions gives the total value of the imaginary part of the SHG.

To have an idea about the origin of the SHG, we have analyzed the spectral features of  $|\chi_{132}^{(2)}(\omega)|$ . A step forward, the absorptive part of the corresponding dielectric function  $\varepsilon_2(\omega)$  as a function of both  $\omega/2$  and  $\omega$  is associated with the spectral structures of  $|\chi_{333}^{(2)}(\omega)|$ , as shown in Fig. 5e. For simplicity, the spectral structures of  $\varepsilon_2(\omega)$ ,  $\varepsilon_2(\omega/2)$  and  $|\chi_{132}^{(2)}(\omega)|$  can be divided into three spectral regions. The spectral region confined between  $E_g/2$  and  $E_g$  is mainly formed by the  $2\omega$  resonance, which is associated with the main spectral structure of  $\varepsilon_2(\omega/2)$ . The second structure between  $E_g$  and 11.0 eV is associated with the interference between  $2\omega$  and  $\omega$  resonances, which is associated with the first spectral structure of  $\varepsilon_2(\omega)$  and the second structure of  $\varepsilon_2(\omega/2)$ . It is clear that in this region the  $\omega$  terms start to oscillate and contribute to the spectral structure of  $|\chi_{132}^{(2)}(\omega)|$  in addition to  $2\omega$  terms. The third spectral structure from 11.0 eV and 13.5 eV is mainly due to  $\omega$  resonance which is associated with the second structure in  $\varepsilon_2(\omega)$ .

Using the obtained value of  $\chi_{ijk}^{(2)}(\omega)$ , we have obtained the values of the microscopic first hyperpolarizability,  $\beta_{ijk}$ ,<sup>68</sup> the vector component along the dipole moment direction, at the static limit, at  $\lambda = 190$  nm and at  $\lambda = 1064$  nm. We should emphasize that the  $\beta_{ijk}$  term cumulatively yields a bulk observable second order susceptibility term,  $\chi_{ijk}^{(2)}(\omega)$ , which in turn is responsible for the strong SHG response.<sup>69</sup> In Table 4, we have presented the value of  $\beta_{132}$  at the static limit and at the wavelengths of 190 nm and 1064 nm.

## 4. Conclusions

A comprehensive *ab initio* calculation was used to investigate the linear and nonlinear optical susceptibility dispersions of  $\text{Li}_3\text{B}_5\text{O}_8(\text{OH})_2$  which crystallizes in a non-centrosymmetric

tetragonal space group. A bulk structure of  $\text{Li}_3\text{B}_5\text{O}_8(\text{OH})_2$  in the form of single crystals is used to investigate the linear and nonlinear optical susceptibility dispersions, taking into account the influence of the packing of structural units on the resulting linear and nonlinear optical susceptibility dispersions. We found that the packing of the  $\text{BO}_3$  structural unit is the main source of the large birefringence, and hence, affects the macroscopic SHG coefficients. The large SHG is due to hyperpolarizability formed by co-parallel  $\text{BO}_3$  triangle groups. The accuracy of the mBJ approach shows that the absorption edge of  $\text{Li}_3\text{B}_5\text{O}_8(\text{OH})_2$  occurs at  $\lambda = 190$  nm and the optical band gap is estimated to be 6.52 eV in good agreement with the experimental data (6.526 eV). Therefore,  $\text{Li}_3\text{B}_5\text{O}_8(\text{OH})_2$  is expected to produce laser radiation in the DUV region. The resulting SHG is 1.5 times that of the well-known NLO crystal  $\text{KH}_2\text{PO}_4$  (KDP) at  $\lambda = 1064$  nm and 3.5 times that of KDP at  $\lambda = 190$  nm.

## Author contribution

A. H. Reshak, as a professor with a PhD in physics and PhD in materials engineering has performed the calculations, analyzed and discussed the results and wrote the manuscript.

## Conflicts of interest

The author declares no competing financial interests.

## Acknowledgements

The result was developed within the CENTEM project, reg. no. CZ.1.05/2.1.00/03.0088, cofunded by the ERDF as part of the Ministry of Education, Youth and Sports OP RDI programme and, in the follow-up sustainability stage, supported through CENTEM PLUS (LO1402) by financial means from the Ministry of Education, Youth and Sports under the National Sustainability Programme I. Computational resources were provided by MetaCentrum (LM2010005) and CERIT-SC (CZ.1.05/3.2.00/08.0144) infrastructures.

## References

- P. A. Franken, G. Weinreich, C. W. Peters and A. E. Hill, Generation of optical harmonics, *Phys. Rev. Lett.*, 1961, 7, 118.
- Y. M. Xu, Y. B. Huang, X. Y. Cui, E. Razzoli, M. Radovic, M. Shi, G. F. Chen, P. Zheng, N. L. Wang and C. L. Zhang, *et al.*, *Nat. Phys.*, 2011, 7, 198–202.
- S. Neil, Ultraviolet lasers, *Nat. Photonics*, 2007, 1, 83–85.
- D. M. Burland, R. D. Miller and C. A. Walsh, Second-Order Nonlinearity in Poled-Polymer Systems, *Chem. Rev.*, 1994, 94, 31–75.
- J. Chiaverini, D. Leibfried, T. Schaez, M. D. Barrett, R. B. Blakestad, J. Britton, W. M. Itano, J. D. Jost, E. Knill

- 1 and C. Langer, *et al.*, Nonlinear optics in the extreme ultraviolet, *Nature*, 2004, **432**, 605–608.
- 6 T. Kiss, F. Kanetaka, T. Yokoya, T. Shimojima, K. Kanai, S. Shin, Y. Onuki, T. Togashi, C. Zhang and C. T. Chen, *et al.*, *Phys. Rev. Lett.*, 2005, **94**, 057001.
- 5 7 L. P. Yatsenko, B. W. Shore, T. Halfmann and K. Bergmann, *Phys. Rev. A: At., Mol., Opt. Phys.*, 1999, **94**, R4237.
- 8 T. Kiss, T. Shimojima, T. Kanaia, T. Yokoya, S. Shin, Y. Onuki, T. Togashi, C. Zhang and C. T. Chen, *J. Electron Spectrosc. Relat. Phenom.*, 2005, **144**, 953–956.
- 10 9 J. Meng, G. Liu, W. Zhang, L. Zhao, H. Liu, X. Jia, D. Mu, S. Liu, X. Dong and J. Zhang, *et al.*, *Nature*, 2009, **462**, 335–338.
- 15 10 G. Balakrishnan, Y. Hu, S. B. Nielsen and T. G. Spiro, *Appl. Spectrosc.*, 2005, **59**, 776–781.
- 11 P. Becker, Borate Materials in Nonlinear Optics, *Adv. Mater.*, 1998, **10**, 979–992.
- 12 X. Jiang, S. Luo, L. Kang, P. Gong, H. Huang, S. Wang, Z. Lin and C. Chen, *ACS Photonics*, 2015, **2**, 1183–1191.
- 20 13 H. Huang, L. Liu, S. Jin, W. Yao, Y. Zhang and C. Chen, *J. Am. Chem. Soc.*, 2013, **135**(49), 18319–18322.
- 14 H. Huang, J. Yao, Z. Lin, X. Wang, R. He, W. Yao, N. Zhai and C. Chen, *Angew. Chem., Int. Ed.*, 2011, **50**, 9141–9144.
- 15 C. T. Chen, T. Sasaki, R. Li, Y. Wu, Z. Lin, Y. Mori, Z. Hu, J. Wang, G. Aka and M. Yoshimura *et al.*, *Nonlinear Optical Borate Crystals Principals and Applications*, Wiley-VCH, New York, NY, USA, 2012.
- 25 16 Y. Yang, X. Jiang, Z. Lin and Y. Wu, *Crystals*, 2017, **7**, 95, DOI: 10.3390/cryst7040095.
- 30 17 H. Yu, H. Wu, S. Pan, Z. Yang, X. Hou, X. Su, Q. Jing, K. R. Poeppelmeier and J. M. Rondinelli, *J. Am. Chem. Soc.*, 2014, **136**, 1264–1267.
- 18 C. T. Chen, J. H. Lu, T. Togashi, T. Suganuma, T. Sekikawa, S. Watanabe, Z. Y. Xu and J. Y. Wang, *Opt. Lett.*, 2002, **27**, 637.
- 35 19 (a) B. C. Wu, D. Y. Tang, N. Ye and C. T. Chen, *Opt. Mater.*, 1996, **5**, 105; (b) C. T. Chen, G. L. Wang, X. Y. Wang and Z. Y. Xu, *Appl. Phys. B: Lasers Opt.*, 2009, **97**, 9.
- 20 R. W. Whatmore, N. M. Shorrocks, C. O'hara, F. W. Ainger and I. M. Young, *Electron. Lett.*, 1981, **17**, 11–12.
- 40 21 (a) H. Konig and R. Hoppe, *Z. Anorg. Allg. Chem.*, 1978, **439**, 71–79; (b) S. Lin, Z. Sun, B. Wu and C. Chen, *J. Appl. Phys.*, 1990, **67**, 634–638.
- 22 K. Byrappa, V. P. Jayantharaia, K. V. K. Shekar, V. Rajeev, V. J. Hanumesh and A. R. Kulkarni, *J. Mater. Sci.*, 1997, **32**, 1599–1602.
- 45 23 ICSD database, [www.fiz-karlsruhe.de/icsd.html](http://www.fiz-karlsruhe.de/icsd.html).
- 24 K. Byrappa and K. V. K. Shekar, *J. Mater. Res.*, 1993, **8**, 864.
- 25 (a) M. Maczka, A. Waskowska, A. Majchrowski, J. Zmija, J. Hanuza, G. A. Peterson and D. A. Keszler, *J. Solid State Chem.*, 2007, **180**, 410–419; (b) P. Li and Z.-H. Liu, *J. Chem. Eng. Data*, 2010, **55**, 2682–2686.
- 50 26 B. C. Wu, D. Y. Tang, N. Ye and C. T. Chen, *Opt. Mater.*, 1996, **5**, 105.
- 55 27 T. Sasaki, Y. Mori, M. Yoshimura, Y. K. Yap and T. Kamimura, *Mater. Sci. Eng.*, 2000, **30**, 1.
- 28 Y. Mori, Y. K. Yap, T. Kamimura, M. Yoshimura and T. Sasaki, *Opt. Mater.*, 2002, **19**, 1.
- 29 T. Kanai, T. Kanda, T. Sekikawa, S. Watanabe, T. Togashi, C. T. Chen, C. Q. Zhang, Z. Y. Xu and J. Y. Wang, *J. Opt. Soc. Am. B*, 2004, **21**, 370.
- 5 30 K. Byrappa, V. P. Jayantharaja, K. V. K. Shekar, V. Rajeev, V. J. Hanumesh, A. R. Kulkarni and A. B. Kulkarni, *J. Mater. Sci.*, 1997, **32**, 1599–1602.
- 31 (a) N. Ye, Q. Chen, B. C. Wu and C. T. Chen, *J. Appl. Phys.*, 1998, **84**, 555–558; (b) C. Chen, N. Ye, J. Lin, J. Jiang, W. R. Zeng and B. C. Wu, *Adv. Mater.*, 1999, **11**, 1071–1078.
- 10 32 M. Abudourehman, L. Wang, X. Zhang, H. Yu, Z. Yang, C. Lei, J. Han and S. Pan, *Inorg. Chem.*, 2015, **54**, 4138–4142.
- 33 P. Blaha, K. Schwarz, G. K. H. Madsen, D. Kvasnicka and J. Luitz, *WIEN2k, An augmented plane wave plus local orbitals program for calculating crystal properties*, Vienna University of Technology, Austria, 2001.
- 15 34 J. P. Perdew, S. Burke and M. Ernzerhof, *Phys. Rev. Lett.*, 1996, **77**, 3865.
- 35 F. Tran and P. Blaha, *Phys. Rev. Lett.*, 2009, **102**, 226401.
- 20 36 [http://www.wien2k.at/reg\\_user/textbooks/usersguide.pdf](http://www.wien2k.at/reg_user/textbooks/usersguide.pdf).
- 37 C. Ambrosch-Draxl and J. O. Sofo, *Comput. Phys. Commun.*, 2006, **175**, 1–14.
- 38 S. Sharma, J. K. Dewhurst and C. Ambrosch-Draxl, *Phys. Rev. B: Condens. Matter Mater. Phys.*, 2003, **67**, 165332.
- 25 39 A. H. Reshak, PhD thesis, Indian Institute of Technology-Roorkee, India, 2005.
- 40 A. H. Reshak, *J. Chem. Phys.*, 2006, **125**, 03471.
- 41 A. H. Reshak, *J. Chem. Phys.*, 2006, **124**, 104707.
- 42 Z. Lin, X. Jiang, L. Kang, P. Gong, S. Luo and M.-H. Lee, *J. Phys. D: Appl. Phys.*, 2014, **47**, 253001.
- 30 43 M. I. Kolinko, I. V. Kityk and A. S. Krochuk, *J. Phys. Chem. Solids*, 1992, **53**, 1315–1320.
- 44 G. E. Davydyuk, O. Y. Khyzhun, A. H. Reshak, H. Kamarudin, G. L. Myronchuk, S. P. Danylchuk, A. O. Fedorchuk, L. V. Piskach, M. Yu. Mozolyuk and O. V. Parasyuk, *Phys. Chem. Chem. Phys.*, 2013, **15**, 6965.
- 35 45 A. H. Reshak, Y. M. Kogut, A. O. Fedorchuk, O. V. Zamuruyeva, G. L. Myronchuk, O. V. Parasyuk, H. Kamarudin, S. Auluck, K. L. Plucinskig and J. Bila, *Phys. Chem. Chem. Phys.*, 2013, **15**, 18979.
- 40 46 V. V. Atuchin, T. A. Gavrilova, J.-C. Grivel and V. G. Kesler, *Surf. Sci.*, 2008, **602**, 3095–3099.
- 47 V. V. Atuchin, T. A. Gavrilova, J.-C. Grivel and V. G. Kesler, *J. Phys. D: Appl. Phys.*, 2009, **42**, 035305.
- 45 48 O. Y. Khyzhun, V. L. Bekenev, V. V. Atuchin, E. N. Galashov and V. N. Shlegel, *Mater. Chem. Phys.*, 2013, **140**, 558–595.
- 49 V. V. Atuchin, E. N. Galashov, O. Y. Khyzhun, V. L. Bekenev, L. D. Pokrovsky, Yu. A. Borovlev and V. N. Zhdankov, *J. Solid State Chem.*, 2016, **236**, 24–31.
- 50 50 H. Huang, X. Li, J. Wang, F. Dong, P. K. Chu, T. Zhang and Y. Zhang, *ACS Catal.*, 2015, **5**(7), 4094–4103.
- 51 H. Huang, X. Han, X. Li, S. Wang, P. K. Chu and Y. Zhang, *ACS Appl. Mater. Interfaces*, 2015, **7**, 482–492.
- 52 A. H. Reshak, *Sci. Rep.*, 2017, **7**, 4615, DOI: 10.1038/srep46415.
- 53 A. H. Reshak and S. Auluck, *RSC Adv.*, 2017, **7**, 14752.

- 1 54 A. H. Reshak and M. G. Brik, *J. Alloys Compd.*, 2016, **675**, 355–363.
- 55 A. H. Reshak, *J. Appl. Phys.*, 2016, **119**, 105706.
- 56 J. W. Lekse, M. A. Moreau, K. L. McNerny, J. Yeon, P. S. Halasyamani and J. A. Aitken, *Inorg. Chem.*, 2009, **48**, 7516–7518.
- 57 J. A. Brant, D. J. Clark, Y. S. Kim, J. I. Jang, J.-H. Zhang and J. A. Aitken, *Chem. Mater.*, 2014, **26**, 3045–3048.
- 58 F. Wu, H. Z. Song, J. F. Jia and X. Hu, *Prog. Nat. Sci.: Mater. Int.*, 2013, **23**(4), 408–412.
- 10 59 Yi Yang, Xingxing Jiang, Zheshuai Lin and Yicheng Wu, *Crystals*, 2017, **7**, 95, DOI: 10.3390/cryst7040095.
- 60 C. T. Chen, T. Sasaki, R. Li, Y. Wu, Z. Lin, Y. Mori, Z. Hu, J. Wang, G. Aka and M. Yoshimura *et al.*, *Nonlinear Optical Borate Crystals Principals and Applications*, Wiley-VCH, New York, NY, USA, 2012.
- 15 61 H. Huang, Y. He, X. Li, M. Li, C. Zeng, F. Dong, X. Du, T. Zhangd and Y. Zhang, *J. Mater. Chem. A*, 2015, **3**, 24547–24556.
- 62 H. Huang, Y. He, Z. Lin, L. Kang and Y. Zhang, *J. Phys. Chem. C*, 2013, **117**, 22986–22994.
- 63 D. R. Penn, *Phys. Rev. B*, 1962, **128**, 2093.
- 64 G. D. Boyd, H. Kasper and J. H. McFee, *IEEE J. Quantum Electron.*, 1971, **7**, 563.
- 5 65 F. Bassani and G. P. Parravicini, *Electronic States and Optical Transitions In Solids*, Pergamon Press Ltd., Oxford, 1975, pp. 149–154.
- 66 C. Ambrosch-Draxl and J. O. Sofo, *Comput. Phys. Commun.*, 2006, **175**, 1–14.
- 10 67 C. T. Chen, Y. B. Wang, B. C. Wu, K. Wu, W. Zeng and L. H. Yu, *Nature*, 1995, **373**, 322.
- 68 R. Y. Boyd, *Principles of Nonlinear Optics*, Academic Press, NY, 1982, p. 420.
- 15 69 R. W. Boyd, *Nonlinear optics*, Academic Press is an imprint of Elsevier, 3rd edn, 2008, ISBN:978-0-12-369470-6.

20

20

25

25

30

30

35

35

40

40

45

45

50

50

55

55